SUPPLEMENTAL FIGURE LEGENDS

Figure S1. Structure of Ku-TLC1$_{KBS}$ and Comparison with Human Ku-dsDNA, Related to Figure 1.

(A) Electron density map of TLC1$_{KBS}$. Stereo view of the Sigma-A weighted 2Fo-Fc map that shows nucleotides 288-312 of TLC1$_{KBS}$ are ordered in the crystal. Refined model of TLC1$_{KBS}$ is superimposed on the electron density map. Contours are drawn at the 1.0 σ level. **(B)** Bar diagram and the structure of Ku70. From the N- to C-termini, the vWA domain, the BBD domain, the insertion, and the CTD motif are colored in light green, green, pink, and dark green, respectively. **(C)** Bar diagram and the structure of Ku80. From the N- to C-termini, the vWA domain, the BBD domain, the insertion, and the CTD motif are colored in light blue, blue, purple, and dark blue, respectively. **(D** and **E)** Structural comparison of yeast Ku70/80-TLC1$_{KBS}$ complex and human Ku70/80-dsDNA Complex. Two orthogonal views of the structure of human Ku70/80-dsDNA complexes (D) and yeast Ku70/80-TLC1$_{KBS}$ complexes (E), respectively.

Figure S2. ITC Measurement of the Interactions between Ku70/80 and Wild-type and Mutant TLC1$_{KBS}$ and Proposed Secondary Structures of TLC1$_{KBS}$ Orthologs, Related to Figure 2.

(A) TLC1$_{KBS}$ (nt 288-312) binds to Ku70/80 equally well as KBS-48nt (nt 278-325) and the mutants of TLC1$_{KBS}$ disrupt or weaker its interaction with Ku70/80, consistent with the Ku70/80-TLC1$_{KBS}$ complex structure analyses. **(B)** Sequence analysis of predicted TLC1$_{KBS}$ RNAs from different yeast species clearly showed that, except for the terminal loop, the sequence of TLC1$_{KBS}$ is highly conserved in the *Saccharomyces* clade.

Figure S3. Structural Analyses of the $Ku80_{vWA}$-$Sir4_{KBM}$ Interaction, Related to Figure 3.

(A and B) Characterization of the interaction between Ku80 and Sir4, and analysis of the mutant $Ku80_{vWA}$-$Sir4_{KBM}$ interactions by yeast two-hybrid assay. Data are average of three independent β-galactosidase measurements. Error bars in the graph represent standard errors of the mean (SEM). **(C)** Electron density map of the $Sir4_{KBM}$ peptide. The Sigma-A weighted 2Fo-Fc map that shows residues 100-115 of $Sir4_{KBM}$ are ordered in the crystal. The refined model of $Sir4_{KBM}$ is superimposed on the electron density map. Contours are drawn at the 1.0 σ level. **(D)** $Sir4_{KBM}$, $TLC1_{KBS}$ and Ku70/80 form a quaternary complex. GST-$Sir4_{KBM}$ was used to pull down Ku70/80 and $TLC1_{KBS}$. Proteins were visualized on SDS-PAGE by Coomassie blue staining, and the $TLC1_{KBS}$ RNA were visualized on 8 M urea PAGE by SYBR® Gold staining. **(E)** ITC measurements of the interactions between wild-type and mutant $Ku80_{vWA}$ and $Sir4_{KBM}$.

Figure S4. Functional Analysis of the $Ku80_{vWA}$-$Sir4_{KBM}$ Interaction, Related to Figure 4.

(A and **B)** Mutants that disrupt Ku80-Sir4 interaction do not show senescence phenotype. A *sir4-null* strain was transformed with *CEN* plasmids expressing either WT or mutant Sir4. The cells were serially re-streaked four times and plated at streak 5 (A). A ku80-null strain was transformed with *CEN* plasmids expressing either wild-type or mutant Ku80. The cells were serially re-streaked for 4 times and plated at streak 5 (B). **(C)** The interaction between Ku80 and Sir4 is required for telomere silencing. Top: Wild-type telomere end protection in strains bearing mutations in

KU80 integrated at the endogenous locus that disrupt the Ku80-Sir4 interaction, as revealed by normal growth at restrictive temperature (37 ˚C). Shown are five-fold serial dilutions of wild-type, mutant, or null strains plated on YPD at 28 ˚C (to monitor plating efficiency) and 37 ˚C. Bottom: Derepression of *URA3* telomeric reporters in strains bearing mutations in *KU80* that disrupt the Ku80-Sir4 interaction integrated at the endogenous locus. Shown are five-fold serial dilutions of wild-type, mutant, or null strains on media lacking uracil (-Ura; to monitor plating efficiency) or containing 5-fluorotic acid (5-FOA), as indicated. **(D)** The interaction between Ku80 and Sir4 is not required for Ku's role in telomere end protection or NHEJ. Wild-type NHEJ in strains bearing mutations in *KU80* that disrupt the Ku80-Sir4 interaction integrated at the endogenous locus, as revealed by growth in the presence of constitutively expressed HO endonuclease (+HO). Shown are five-fold serial dilutions of wild-type, mutant, or null strains plated on YPD (to monitor plating efficiency) and YPGal, as indicated.

Figure S5. Primary Sequence Analysis of Est1 Proteins and Characterization of *Kl*Cdc13$_{EBM}$, Related to Figure 5.

(A) Multiple sequence alignment of Est1 family members. The secondary structures (α, α-helix; β, α-strand; η, 3_{10}-helix) of *Kl*Est1 are labeled on the top of each bars. Conserved residues are boxed and highlighted in red. **(B)** Protein folding analysis of *Sc*Est1 and *Kl*Est1 by the PONDR-Fit program. The analysis results show that the C-terminal regions of most Est1 proteins are disordered. **(C)** ITC measurement of the interactions between *Kl*Est1 and different fragments of *Kl*Cdc13 within *Kl*Cdc13$_{RD}$.

Figure S6. Crystallographic and mutational analyses of the *Kl*Est1-*Kl*Cdc13$_{EBM}$ interaction, Related to Figure 5.

(A) Electron density map of the *Kl*Cdc13$_{EBM}$ peptide in the *Kl*Est1-*Kl*Cdc13$_{EBM}$ complex. Stereo view of the Sigma-A weighted 2Fo-Fc map that shows of *Kl*Cdc13$_{EBM-N}$ (residues 213-222) and *Kl*Cdc13$_{EBM-C}$ (residues 232–238) of *Kl*Cdc13$_{EBM}$ are ordered in the crystal. Refined models of *Kl*Cdc13$_{EBM-N}$ and *Kl*Cdc13$_{EBM-C}$ are superimposed on the electron density map. Contours are drawn at the 1.0 σ level. **(B)** ITC measurement of the wild-type and mutant *Kl*Est1-*Kl*Cdc13$_{EBM}$ interactions.

Figure S7. Functional Analysis of the *Kl*Est1-*Kl*Cdc13$_{EBM}$ Interaction, Related to Figure 6.

(A) Mutations in Cdc13$_{EBM-N}$ do not show senescence phenotype. A *CDC13/cdc13Δ* diploid strain was transformed with *CEN CDC13* (or mutant *cdc13*), and then was sporulated and dissected. Cells were taken from serial streaks 2, 4, 6 and 8. **(B)** Cdc13-F237A and -E252K mutant proteins are expressed at the wild-type level. Upper panel: Myc-tagged Cdc13-WT, -F237A, and -E252K proteins were ectopically expressed under control of the native Cdc13 promoter using a *CEN* vector introduced into the *cdc13Δ* strain. The expression level was verified by quantitative western blot using anti-Myc antibody and IRDye conjugated secondary antibody. Wild-type Cdc13 protein with identical 18xMyc tag expressed from native genomic locus served as endogenous control. Fluorescence signal in the linear range was normalized to that of the loading control. Lower panel: Mean expression levels for three independent clones of each strain are plotted, the error bars are SEM. **(C)** Cdc13-F237A and -E252K Mutant Proteins Exhibit Nearly Wild-type Level of Telomere Binding. Cdc13-

Myc ChIP-qPCR assay performed with asynchronous yeast cultures using the complementation system described in (B). The mean values of % input recovered for three independent clones for each strain are plotted. The error bars are SEM. *ARO1* is a non-telomeric locus control. IgG control for non-specific binding was performed with the *CDC13-WT* strain. **(D)** Disruption of both the TLC1-Ku70/80-Sir4 and the Est1-Cdc13 pathways resulted in critically short telomeres. Measurement of average telomere length of yeast strains shown in Figure 6C and 6D taken from streak 6 (wild-type, $cdc13^{F237A}$ and $tlc1^{\Delta AU}$) or streak 4 (for strains with senescence phenotype). Telomere length was calculated from three independent experiments (mean ± SEM).

Figure S1

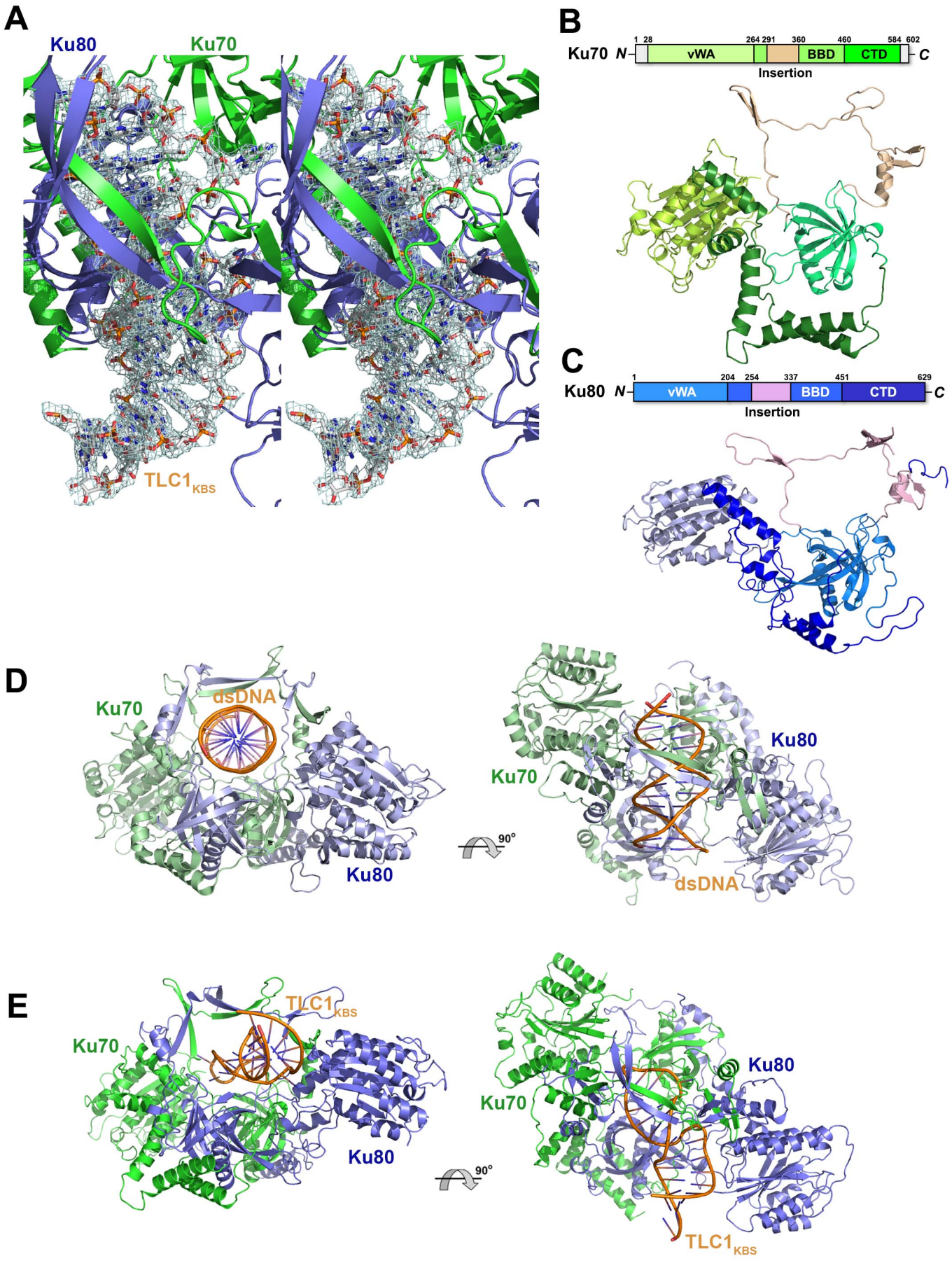
A
Ku80
Ku70
TLC1KBS
B
Ku70 N
1 28
264 291
360
460
584 602
vWA
BBD
CTD
C
Insertion
C
Ku80 N
1
204 254
337
451
629
vWA
BBD
CTD
C
Insertion
D
Ku70
dsDNA
Ku80
90°
Ku70
Ku80
dsDNA
E
TLC1KBS
Ku70
Ku80
90°
Ku80
Ku70
TLC1KBS

Figure S2

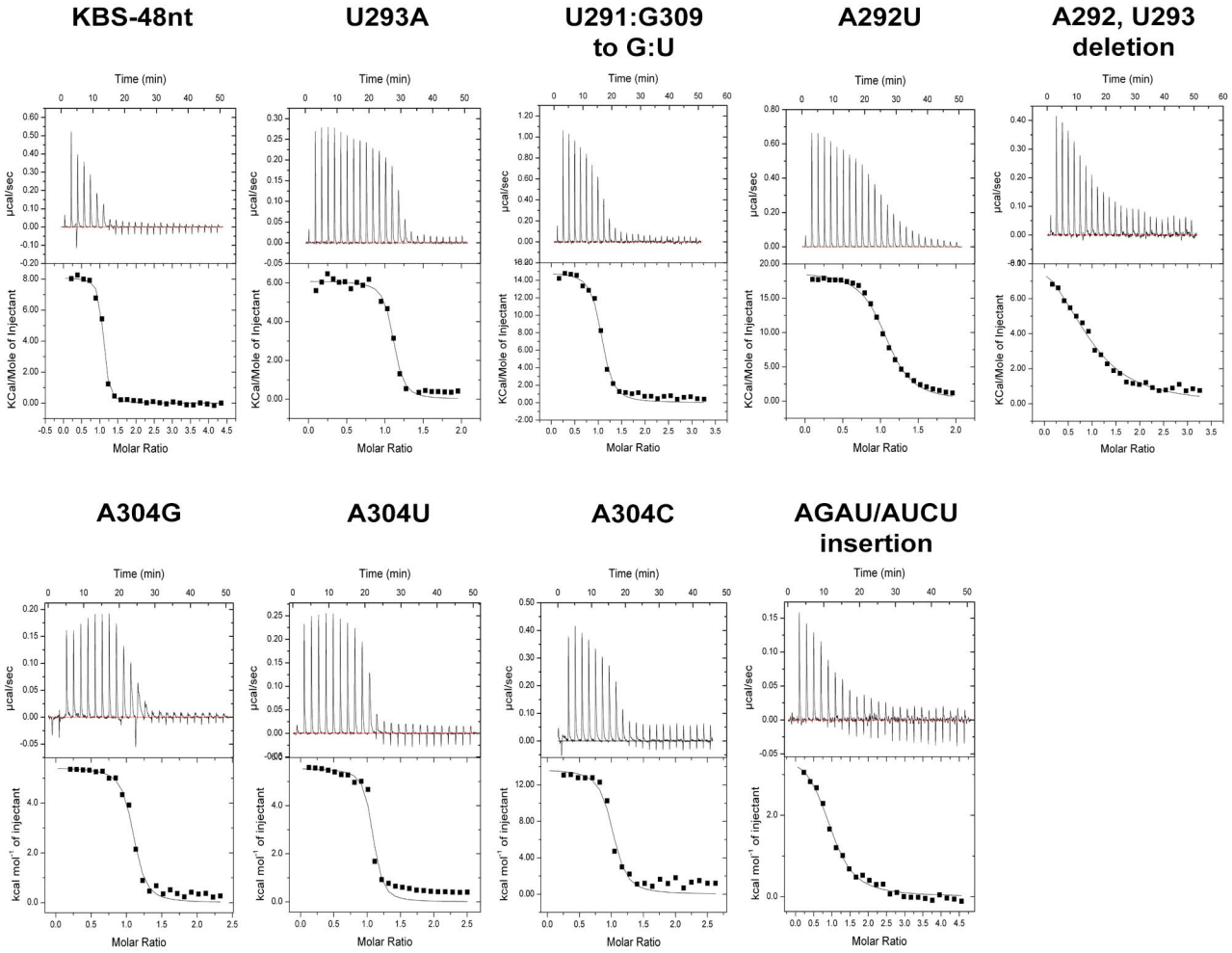
KBS-48nt
U293A
U291:G309 to G:U
A292U
A292, U293 deletion
A304G
A304U
A304C
AGAU/AUCU insertion
Time (min)
µcal/sec
KCal/Mole of Injectant
kcal mol⁻¹ of injectant
Molar Ratio

Figure S3

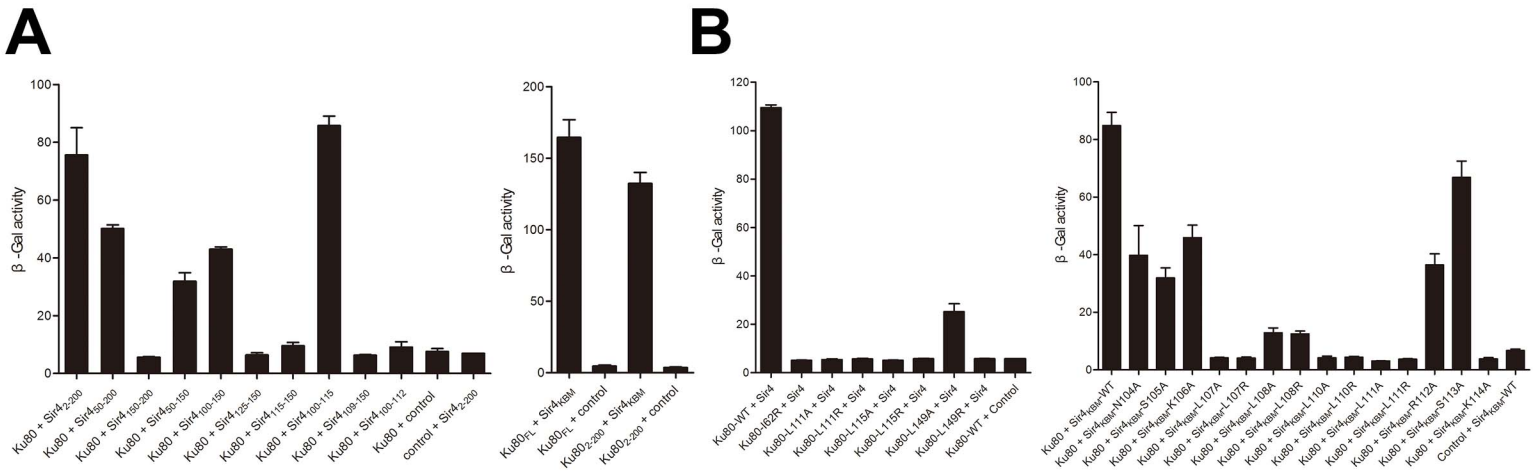
A
B
β -Gal activity
Ku80 + Sir4 2-200
Ku80 + Sir4 50-200
Ku80 + Sir4 150-200
Ku80 + Sir4 50-150
Ku80 + Sir4 100-150
Ku80 + Sir4 125-150
Ku80 + Sir4 100-115
Ku80 + Sir4 100-150
Ku80 + Sir4 100-112
Ku80 + control
control + Sir4 2-200
Ku80 FL + Sir4 KBM
Ku80 FL + control
Ku80 2-200 + Sir4 KBM
Ku80 2-200 + control
Ku80-WT + Sir4
Ku80-I62R + Sir4
Ku80-L111A + Sir4
Ku80-L111R + Sir4
Ku80-L115A + Sir4
Ku80-L115R + Sir4
Ku80-L149A + Sir4
Ku80-L149R + Sir4
Ku80-WT + Control
Ku80 + Sir4 KBM-WT
Ku80 + Sir4 KBM-N104A
Ku80 + Sir4 KBM-S105A
Ku80 + Sir4 KBM-K106A
Ku80 + Sir4 KBM-L107A
Ku80 + Sir4 KBM-L107R
Ku80 + Sir4 KBM-L108A
Ku80 + Sir4 KBM-L108R
Ku80 + Sir4 KBM-L110A
Ku80 + Sir4 KBM-L110R
Ku80 + Sir4 KBM-L111A
Ku80 + Sir4 KBM-L111R
Ku80 + Sir4 KBM-R112A
Ku80 + Sir4 KBM-S113A
Ku80 + Sir4 KBM-K114A
Control + Sir4 KBM-WT

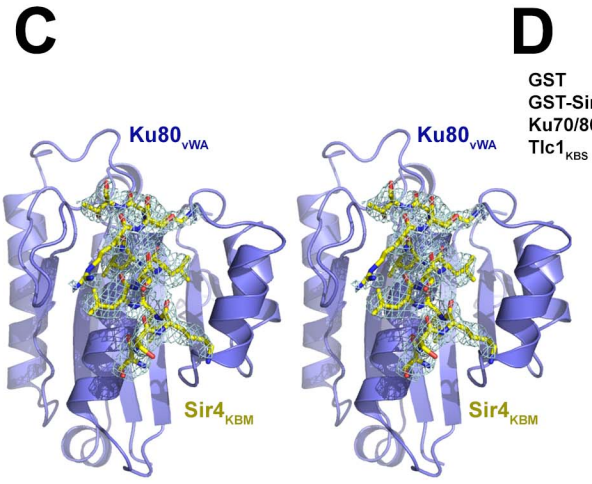
C
Ku80 vWA
Sir4 KBM
Ku80 vWA
Sir4 KBM

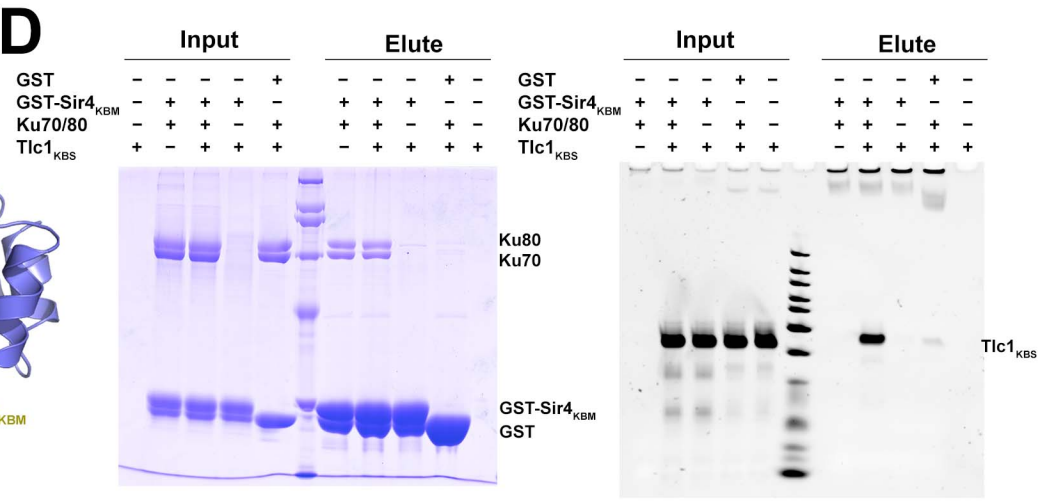
D
Input
Elute
GST
GST-Sir4 KBM
Ku70/80
Tlc1 KBS
Ku80
Ku70
GST-Sir4 KBM
GST
Tlc1 KBS

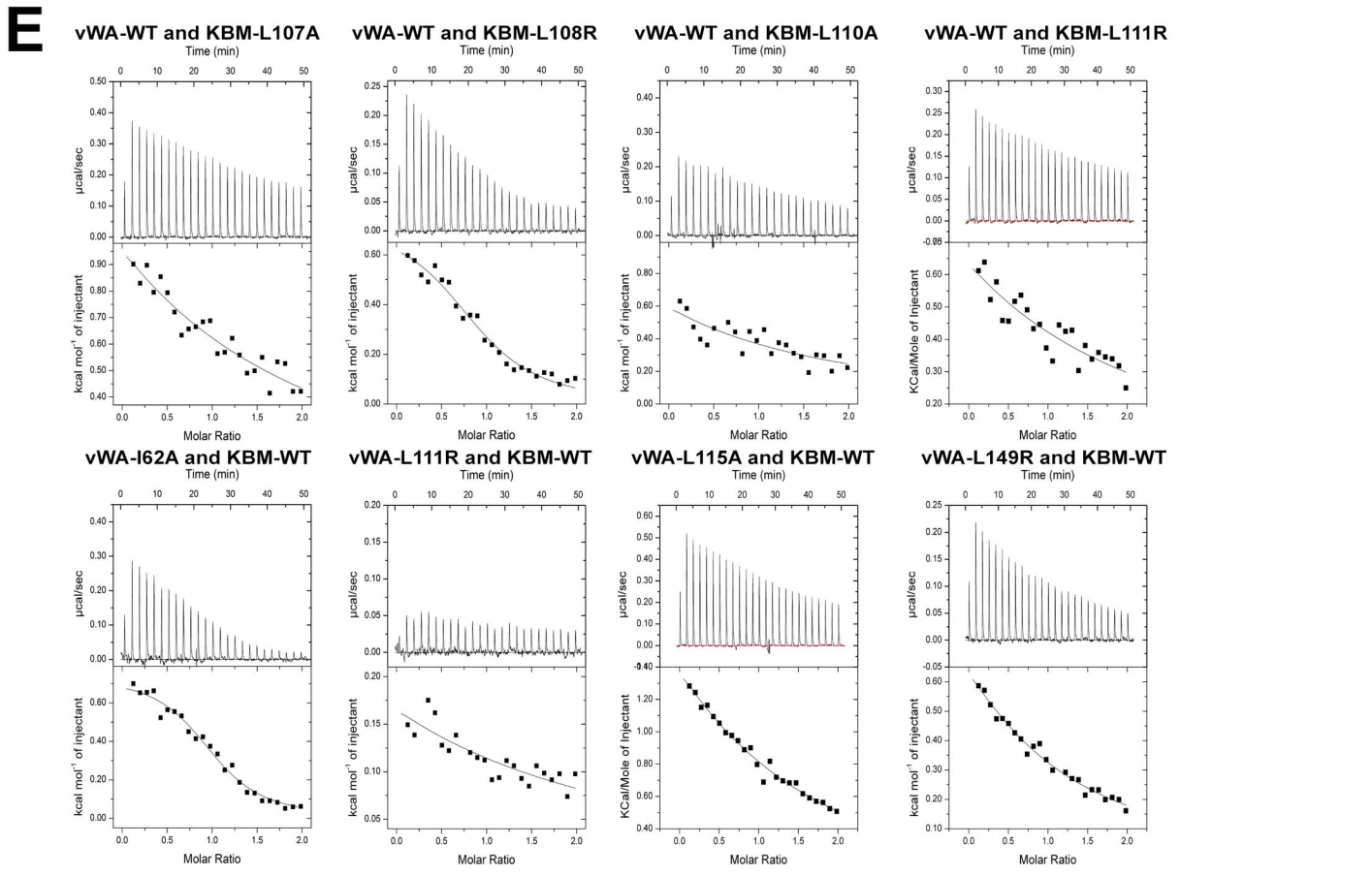
E
vWA-WT and KBM-L107A
vWA-WT and KBM-L108R
vWA-WT and KBM-L110A
vWA-WT and KBM-L111R
vWA-I62A and KBM-WT
vWA-L111R and KBM-WT
vWA-L115A and KBM-WT
vWA-L149R and KBM-WT
Time (min)
µcal/sec
kcal mol-1 of injectant
KCal/Mole of Injectant
Molar Ratio

Figure S4

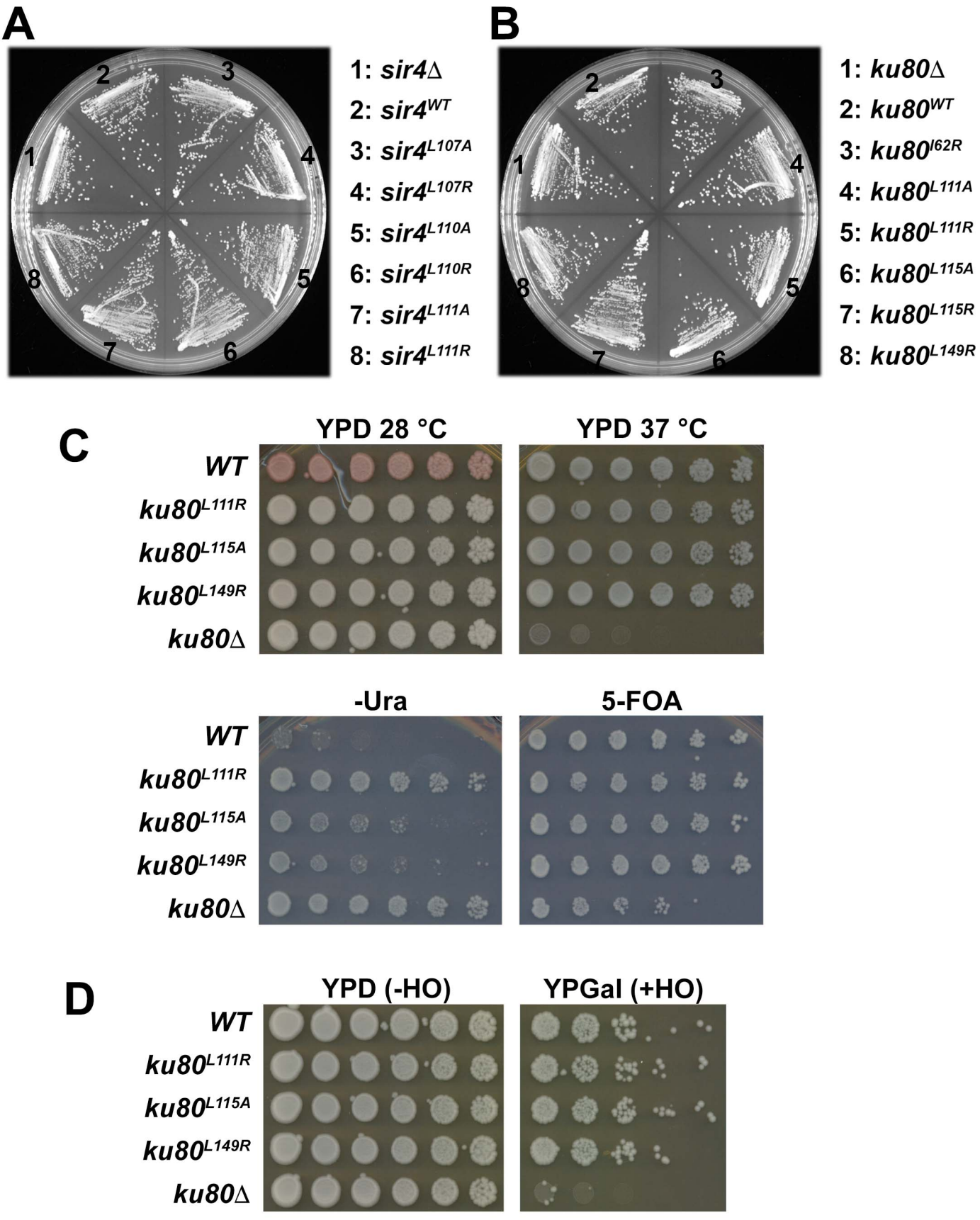
A
1: sir4Δ
2: sir4WT
3: sir4L107A
4: sir4L107R
5: sir4L110A
6: sir4L110R
7: sir4L111A
8: sir4L111R
B
1: ku80Δ
2: ku80WT
3: ku80I62R
4: ku80L111A
5: ku80L111R
6: ku80L115A
7: ku80L115R
8: ku80L149R
C
YPD 28 °C
YPD 37 °C
WT
ku80L111R
ku80L115A
ku80L149R
ku80Δ
-Ura
5-FOA
D
YPD (-HO)
YPGal (+HO)

Figure S5

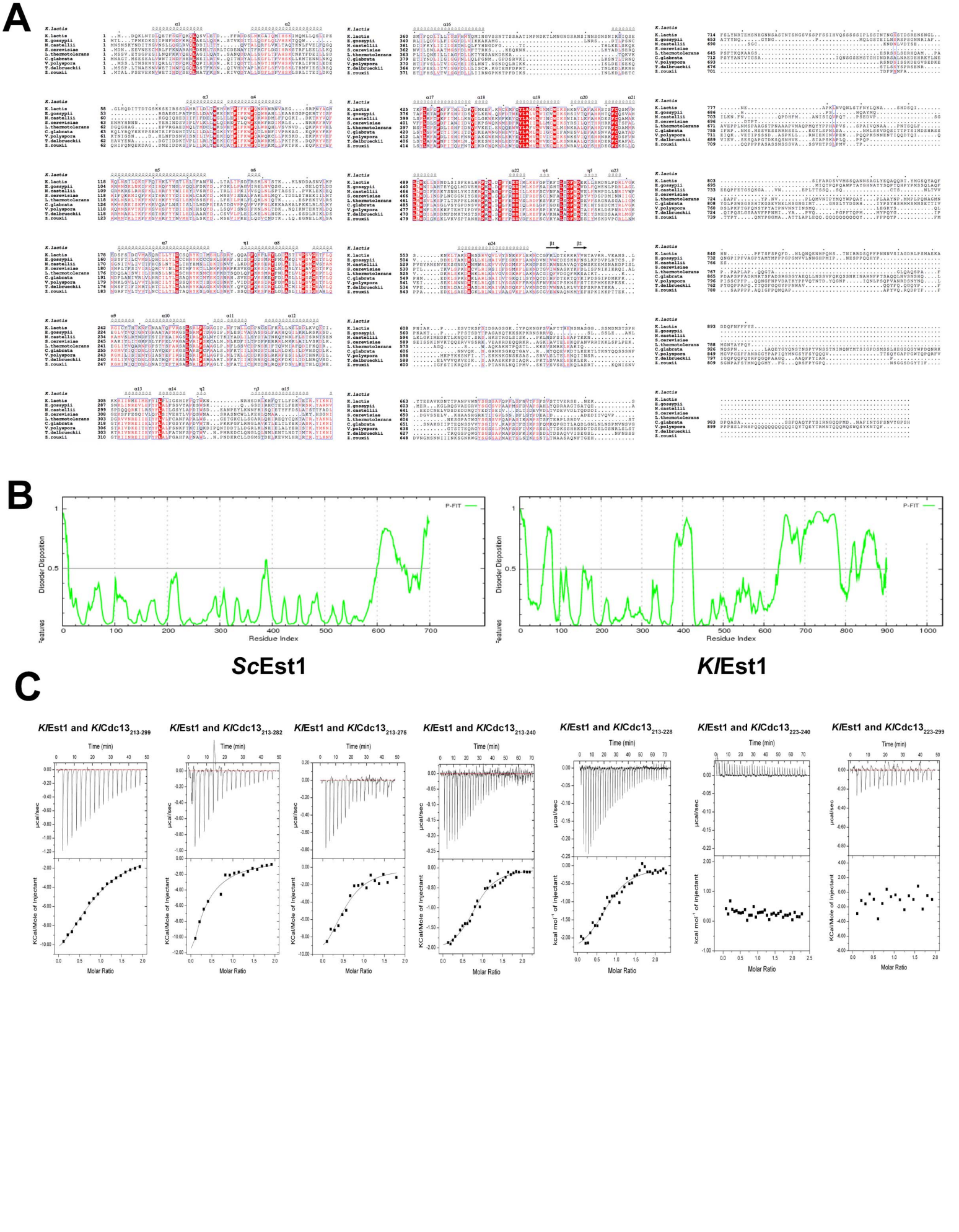
A
B
ScEst1
KlEst1
C
KlEst1 and KlCdc13213-299
KlEst1 and KlCdc13213-282
KlEst1 and KlCdc13213-275
KlEst1 and KlCdc13213-240
KlEst1 and KlCdc13213-228
KlEst1 and KlCdc13223-240
KlEst1 and KlCdc13223-299
Time (min)
Molar Ratio
Residue Index
P-FIT
Disorder Disposition

Figure S6

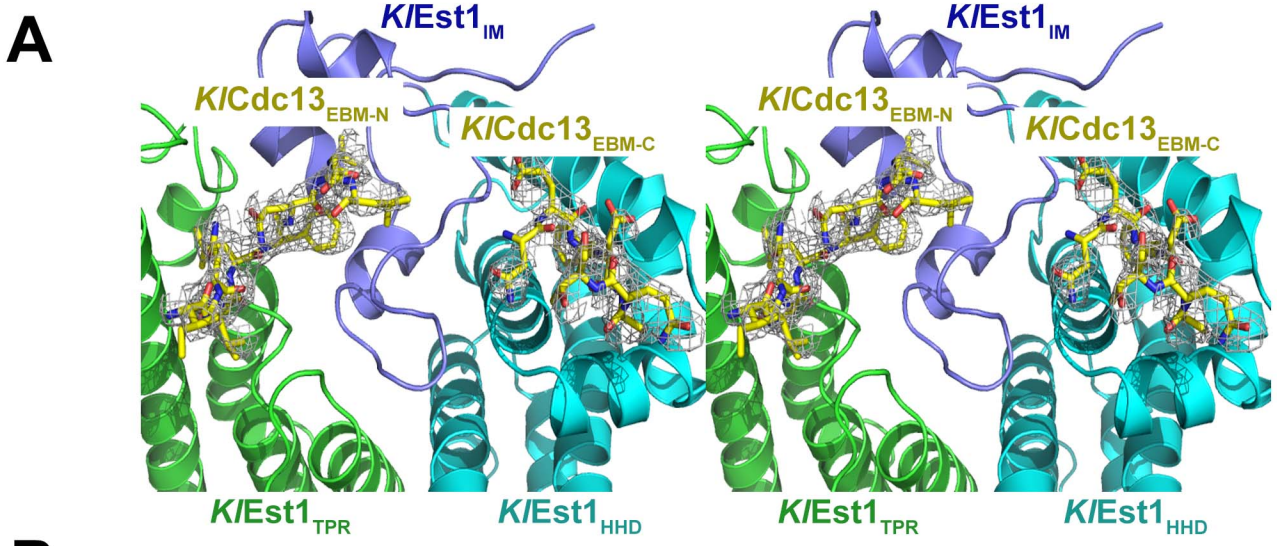
A
KlEst1IM
KlCdc13EBM-N
KlCdc13EBM-C
KlEst1TPR
KlEst1HHD
KlEst1IM
KlCdc13EBM-N
KlCdc13EBM-C
KlEst1TPR
KlEst1HHD

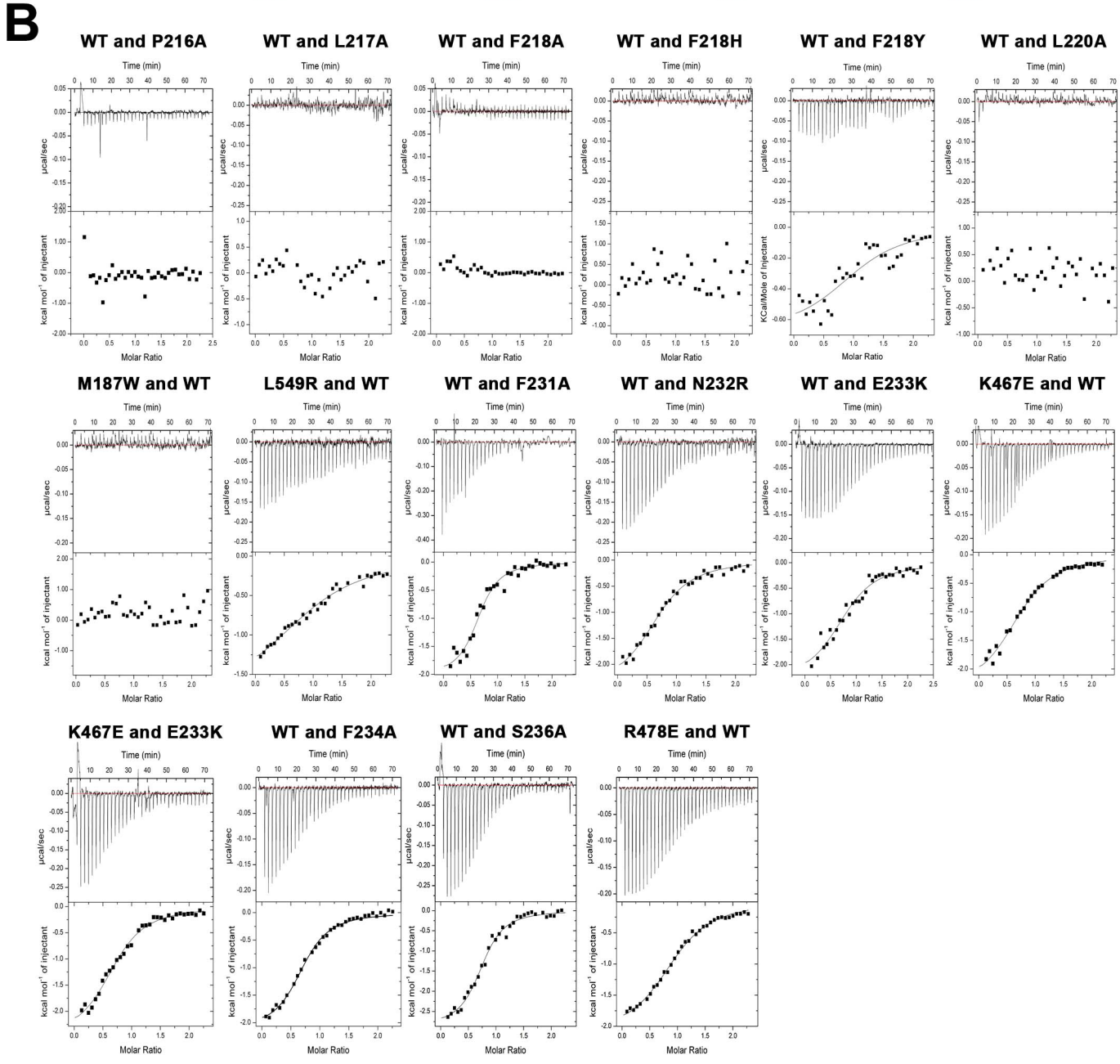
B
WT and P216A
WT and L217A
WT and F218A
WT and F218H
WT and F218Y
WT and L220A
M187W and WT
L549R and WT
WT and F231A
WT and N232R
WT and E233K
K467E and WT
K467E and E233K
WT and F234A
WT and S236A
R478E and WT
Time (min)
µcal/sec
kcal mol⁻¹ of injectant
KCal/Mole of injectant
Molar Ratio

Figure S7

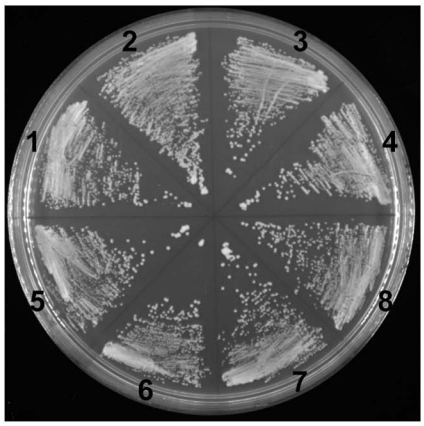

1: *cdc13*^{WT} ×2
2: *cdc13*^{WT} ×4
3: *cdc13*^{WT} ×6
4: *cdc13*^{WT} ×8
5: *cdc13*^{P235A} ×2
6: *cdc13*^{P235A} ×4
7: *cdc13*^{P235A} ×6
8: *cdc13*^{P235A} ×8

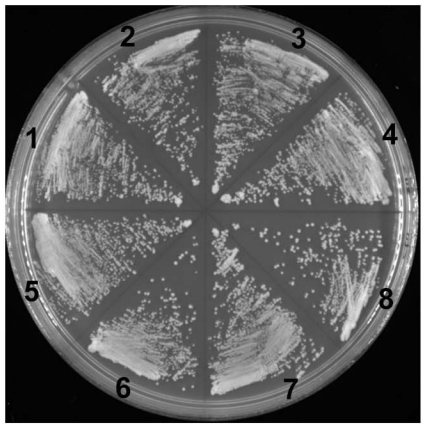

1: *cdc13*^{F237A} ×2
2: *cdc13*^{F237A} ×4
3: *cdc13*^{F237A} ×6
4: *cdc13*^{F237A} ×8
5: *cdc13*^{F237H} ×2
6: *cdc13*^{F237H} ×4
7: *cdc13*^{F237H} ×6
8: *cdc13*^{F237H} ×8

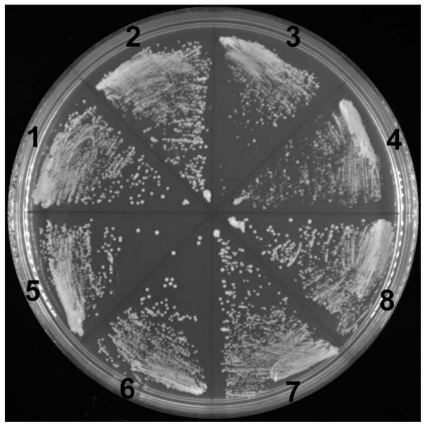

1: *cdc13*^{F237Y} ×2
2: *cdc13*^{F237Y} ×4
3: *cdc13*^{F237Y} ×6
4: *cdc13*^{F237Y} ×8
5: *cdc13*^{P239A} ×2
6: *cdc13*^{P239A} ×4
7: *cdc13*^{P239A} ×6
8: *cdc13*^{P239A} ×8

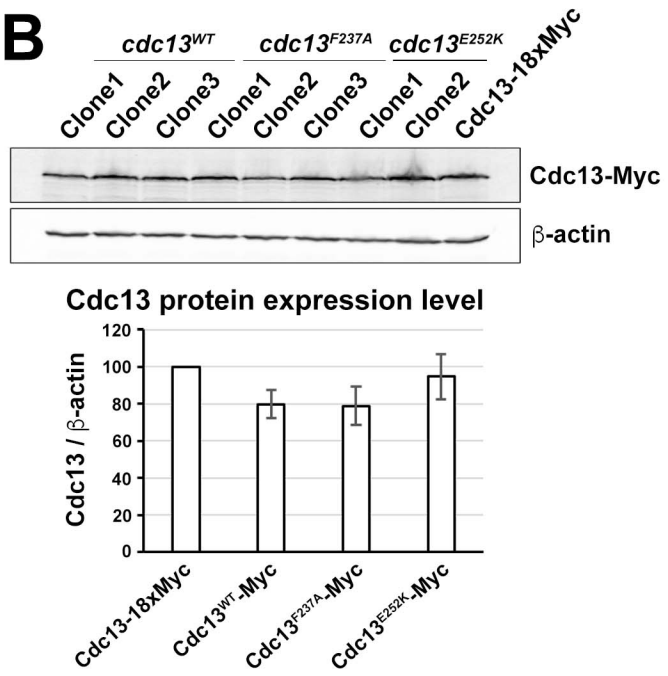

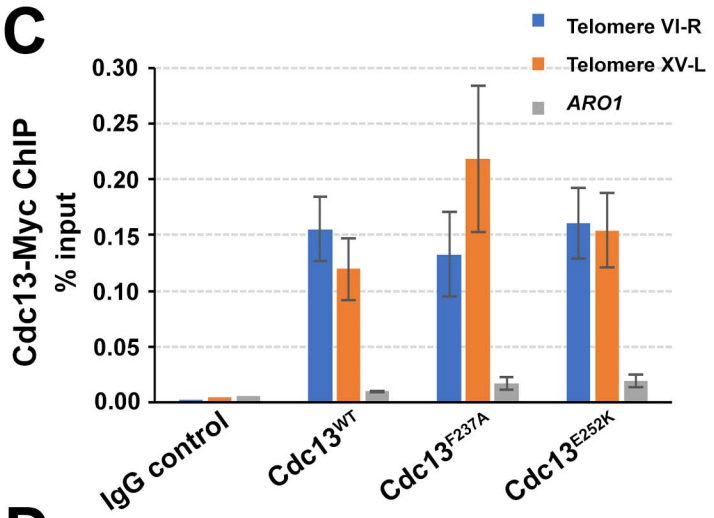

Genotype	Decrease in telomere length (bp)
WT	0
cdc13^{F237A}	~220
tlc1$^{\Delta AU}$	~130
cdc13^{F237A} + *tlc1*$^{\Delta AU}$	~300 (senesced)
cdc13^{F237A} + *sir4*Δ	~300 (senesced)
cdc13^{F237A} + *sir4*^{WT}	~280
cdc13^{F237A} + *sir4*^{L107A}	~290 (senesced)
cdc13^{F237A} + *sir4*^{L111R}	~290 (senesced)
cdc13^{F237A} + *ku80*^{WT}	~220
cdc13^{F237A} + *ku80*^{L111R}	~290 (senesced)
cdc13^{F237A} + *ku80*^{L115A}	~290 (senesced)

Table S1. Crystal Data Collection and Refinement Statistics, Related to Figure 1

	Ku70/80_TLC1$_{KBS}$ (Native)	Ku70/80_TLC1$_{KBS}$ (SeMet-SAD)
Data collection		
Wavelength (Å)	0.97853	0.97853
Space group	*P*1	*P*1
Cell dimensions		
a, b, c (Å)	116.3, 115.2, 115.8	115.4, 114.2, 115.1
α, β, γ (°)	77.4, 78.4, 63.7	77.6, 78.7, 63.9
Resolution (Å)	2.8	3.2
R_{merge} (%)	7.6 (55.6) *	9.3 (61.3) *
$I / \sigma I$	16.3 (2.6) *	12.6 (2.0) *
Completeness (%)	93.9 (96.0) *	98.8 (98.6) *
Redundancy	3.8 (3.8) *	23.5 (4.5) *
Refinement		
Resolution (Å)	44.11-2.80	
No. of reflections	118,137	
R_{work} / R_{free} (%)	21.5/25.8	
No. of atoms		
Ku70	13,647	
Ku80	13,444	
Tlc1$_{KBS}$	1,923	
Water	306	
B-factors (Å^2)		
Ku70	61.1	
Ku80	77.7	
Tlc1$_{KBS}$	63.9	
Water	40.9	
R.m.s. deviations		
Bond lengths (Å)	0.003	
Bond angles (°)	0.587	
Ramanchandran plot		
Favored region	97.3%	
Allowed region	100.0%	
Outlier region	0.0%	

*Highest resolution shell is shown in parenthesis

Table S2. Crystal Data Collection and Refinement Statistics, Related to Figure 3

	$Ku80_{vWA}$_$Sir4_{KBM}$ (Native)	$Ku80_{vWA}$_$Sir4_{KBM}$ (SeMet-SAD)
Data collection		
Wavelength (Å)	0.97851	0.97851
Space group	$P3_121$	$P3_221$
Cell dimensions		
a, b, c (Å)	79.5, 79.5, 82.9	79.2, 79.2, 165.7
α, β, γ (°)	90.0, 90.0, 120.0	90.0, 90.0, 120.0
Resolution (Å)	2.4	2.8
R_{merge} (%)	7.1 (88.8) *	10.9 (76.9) *
I / σI	48.0 (1.8) *	24.6 (2.0) *
Completeness (%)	99.6 (96.2) *	99.7 (99.9) *
Redundancy	18.0 (11.4) *	19.1 (12.0) *
Refinement		
Resolution (Å)	27.64-2.40	
No. of reflections	10,957	
R_{work} / R_{free} (%)	20.1/24.8	
No. of atoms		
$Ku80_{vWA}$	1,498	
$Sir4_{KBM}$	94	
Ion	5	
Water	35	
B-factors (Å^2)		
$Ku80_{vWA}$	28.7	
$Sir4_{KBM}$	44.4	
Ion	66.3	
Water	23.9	
R.m.s. deviations		
Bond lengths (Å)	0.010	
Bond angles (°)	1.306	
Ramanchandran plot		
Favored region	98.4%	
Allowed region	100.0%	
Outlier region	0.0%	

*Highest resolution shell is shown in parenthesis

Table S3. Crystal Data Collection and Refinement Statistics, Related to Figure 5

	*Kl*Est1_*Kl*Cdc13$_{EBM}$ (Native)	*Kl*Est1_*Kl*Cdc13$_{EBM}$ (SeMet-SAD)
Data collection		
Wavelength (Å)	0.97860	0.97860
Space group	*C*2	*C*2
Cell dimensions		
a, b, c (Å)	108.6, 41.7, 147.1	112.7, 42.5, 150.9
α, β, γ (°)	90.0, 97.5, 90.0	90.0, 98.0, 90.0
Resolution (Å)	2.2	2.5
R_{merge} (%)	10.1 (59.4) *	11.3 (76.0) *
$I / \sigma I$	18.2 (1.9) *	33.3 (2.2) *
Completeness (%)	91.8 (93.6) *	94.7 (95.3) *
Redundancy	6.3 (5.8) *	13.3 (11.8) *
Refinement		
Resolution (Å)	40.86-2.20	
No. of reflections	30,684	
R_{work} / R_{free} (%)	17.6/22.5	
No. of atoms		
Est1	4,233	
Cdc13$_{EBM}$	136	
Water	73	
B-factors (Å^2)		
Est1	65.4	
Cdc13$_{EBM}$	89.0	
Water	53.8	
R.m.s. deviations		
Bond lengths (Å)	0.005	
Bond angles (°)	0.852	
Ramanchandran plot		
Favored region	99.0%	
Allowed region	100.0%	
Outlier region	0.0%	

*Highest resolution shell is shown in parenthesis

Table S4. Plasmids Used for This Study, Related to STAR Methods

Plasmid Name	Description	Source
pRS315	*CEN LEU2*	Gift from JQ Zhou
pRS316	*CEN URA3*	Gift from JQ Zhou
pRS415	*CEN LEU2*	Gift from JQ Zhou
pRS303-*est1Δ*	YIp *HIS3 est1Δ*	Gift from JQ Zhou
pVL1107	*CEN LEU2 CDC13-EST2 fusion*	Gift from JQ Zhou
pCH249	*CEN LEU2 cdc13-2-EST2 fusion*	pVL1107
pCH253	*CEN URA3 EST1*	This study
pCH254	*CEN URA3 est1-60*	pCH253
pRS305-*tlc1Δ*	YIp *LUE2 tlc1Δ*	Gift from JQ Zhou
pRS303-*tlc1Δ*	YIp *HIS3 tlc1Δ*	pRS305-*tlc1Δ*
pRS316-*TLC1*	*CEN URA3 TLC1*	Gift from JQ Zhou
pRS316-*tlc1Δ48*	*CEN URA3 tlc1Δ48*	Gift from JQ Zhou
pCH414	*CEN URA3 tlc1ΔAU*	pRS315-*TLC1*
pCH198	*CEN URA3 CDC13*	This study
pCH323	*CEN LUE2 CDC13*	This study
pCH324	*CEN LEU2 cdc13-P235A*	pCH323
pCH325	*CEN LEU2 cdc13-F237A*	pCH323
pCH326	*CEN LEU2 cdc13-E252K*	pCH323
pCH327	*CEN LEU2 cdc13-F253A*	pCH323
pCH328	*CEN LEU2 cdc13-S255A*	pCH323
pCH395	*CEN LEU2 cdc13-F237H*	pCH323
pCH396	*CEN LEU2 cdc13-F237Y*	pCH323
pCH397	*CEN LEU2 cdc13-P239A*	pCH323
pCH407	YIp *HIS3 sir4Δ*	This study
pCH408	*CEN URA3 SIR4*	This study
pCH416	*CEN URA3 sir4-L107R*	pCH408
pCH420	*CEN URA3 sir4-L111R*	pCH408
pRS303-*ku80Δ*	YIp *HIS3 ku80Δ*	Gift from JQ Zhou
pCH410	*CEN LEU2 KU80*	This study
pCH427	*CEN LEU2 ku80-L111R*	pCH410
pCH428	*CEN LEU2 ku80-L115A*	pCH410
pMLW323	*CEN LEU2 CDC13*	This study
pMLW324	*CEN LEU2 cdc13-F237A*	pMLW323
pMLW325	*CEN LEU2 cdc13-E252K*	pMLW323

Table S5. Yeast Strains Used for This Study, Related to STAR Methods

Strain Name	Genotype	Source
yCH001	*MATa/α his3Δ1/his3Δ1 leu2Δ0/leu2Δ0 LYS2/lys2Δ0 met15Δ0/MET15 ura3Δ0/ura3Δ0 CDC13/cdc13Δ::Kanr*	Euroscarf, SRD GmbH
yCH002	*MATa/α his3Δ1/his3Δ1 leu2Δ0/leu2Δ0 LYS2/lys2Δ0 met15Δ0/MET15 ura3Δ0/ura3Δ0 CDC13/cdc13Δ::kanr EST1/est1Δ::HIS3*	yCH001
yCH005	*MATα (or MATa) his3Δ1 leu2Δ0 lys2Δ0 (or met15Δ0) ura3Δ0 cdc13Δ::kanr pCH198(CEN URA3 CDC13)*	yCH001
yCH051	*MATa/α his3Δ1/his3Δ1 leu2Δ0/leu2Δ0 LYS2/lys2Δ0 met15Δ0/MET15 ura3Δ0/ura3Δ0 CDC13/cdc13Δ::kanr KU80/ku80Δ::HIS3*	yCH001
yCH052	*MATa/α his3Δ1/his3Δ1 leu2Δ0/leu2Δ0 LYS2/lys2Δ0 met15Δ0/MET15 ura3Δ0/ura3Δ0 CDC13/cdc13Δ::kanr TLC1/tlc1Δ::HIS3*	yCH001
yCH133	*MATα his3Δ1 leu2Δ0 lys2Δ0 ura3Δ0 ku80Δ::kanr*	Euroscarf, SRD GmbH
yCH134	*MATα his3Δ1 leu2Δ0 lys2Δ0 ura3Δ0 sir4Δ::kanr*	Euroscarf, SRD GmbH
yCH143	*MATα (or MATa) his3Δ1 leu2Δ0 lys2Δ0 (or met15Δ0) ura3Δ0 cdc13Δ::kanr sir4Δ::HIS3 pCH198(CEN URA3 CDC13)*	yCH005
yDZ651	*MATα (or MATa) his3Δ1 leu2Δ0 lys2Δ0 (or met15Δ0) ura3Δ0 cdc13Δ::kanr sir4Δ::HIS3 pCH198(CEN URA3 CDC13) EST2-Gly8-myc13::LYS2*	yCH143
UCC3505	*MATα ura3-52 lys2-801 ade2-101 trp1-Δ63 his3-Δ200 leu2-Δ1 ppr1::HIS3 adh4::URA3-(URA3* at TEL VIIL*) DIA5-1 (ADE2* at TEL VR*)*	Singer and Gottschling, 1994
YVL885	*MATα yku80-Δ::kan^r ura3-52 lys2-801 ade2-101 trp1-Δ63 his3-Δ200 leu2-Δ1 ppr1::HIS3 adh4::URA3-(URA3* at TEL VIIL*) DIA5-1 (ADE2* at TEL VR*)*	Bertuch and Lundblad, 2003
YAB1010	*MAT***a** *yku80-L111R ura3-52 lys2-801 ade2-101 trp1-Δ63 his3-Δ200 leu2-Δ1 ppr1::HIS3 adh4::URA3-(URA3* at TEL VIIL*) DIA5-1 (ADE2* at TEL VR*)*	UCC3505
YAB1011	*MATα yku80-L115A ura3-52 lys2-801 ade2-101 trp1-Δ63 his3-Δ200 leu2-Δ1 ppr1::HIS3 adh4::URA3-(URA3* at TEL VIIL*) DIA5-1 (ADE2* at TEL VR*)*	UCC3505
YAB1012	*MATα yku80-L149R ura3-52 lys2-801 ade2-101 trp1-Δ63 his3-Δ200 leu2-Δ1 ppr1::HIS3 adh4::URA3-(URA3* at TEL VIIL*) DIA5-1 (ADE2* at TEL VR*)*	UCC3505

JKM139	*MATα hml-Δ::ADE1 hmr-Δ::ADE1 ade1-110 leu2,3-112 lys5 trp1-Δ::hisG ura3-52 ade3::GAL10 HO*	Lee *et al.*, 1998
YAB795	*MATα yku80-Δ::kan^r YKU70-TAF hml-Δ::ADE1 hmr-Δ::ADE1 ade1-110 leu2,3-112 lys5 trp1-Δ::hisG ura3-52 ade3::GAL10 HO*	JKM139
YAB1013	*MATα yku80-L111R hml-Δ::ADE1 hmr-Δ::ADE1 ade1-110 leu2,3-112 lys5 trp1-Δ::hisG ura3-52 ade3::GAL10 HO*	JKM139
YAB1014	*MATα yku80-L115A hml-Δ::ADE1 hmr-Δ::ADE1 ade1-110 leu2,3-112 lys5 trp1-Δ::hisG ura3-52 ade3::GAL10 HO*	JKM139
YAB1015	*MATα yku80-L149R hml-Δ::ADE1 hmr-Δ::ADE1 ade1-110 leu2,3-112 lys5 trp1-Δ::hisG ura3-52 ade3::GAL10 HO*	JKM139
	MATa his3Δ1 leu2Δ0 LYS2 ura3Δ0 cdc13Δ::Kanr pMLW323 (CEN LEU2 CDC13) Est1-13Myc::TRP1	yCH001
	MATa his3Δ1 leu2Δ0 LYS2 ura3Δ0 cdc13Δ::Kanr pMLW325 (CEN LEU2 cdc13-F237A) Est1-13Myc::TRP1	yCH001
	MATa his3Δ1 leu2Δ0 LYS2 ura3Δ0 cdc13Δ::Kanr pMLW326 (CEN LEU2 cdc13-E252K) Est1-13Myc::TRP1	yCH001
	MATa his3Δ1 leu2Δ0 LYS2 ura3Δ0 cdc13Δ::Kanr pMLW323 (CEN LEU2 CDC13) Est2-13Myc::TRP1	yCH001
	MATa his3Δ1 leu2Δ0 LYS2 ura3Δ0 cdc13Δ::Kanr pMLW325 (CEN LEU2 cdc13-F237A) Est2-13Myc::TRP1	yCH001
	MATa his3Δ1 leu2Δ0 LYS2 ura3Δ0 cdc13Δ::Kanr pMLW326 (CEN LEU2 cdc13-E252K) Est2-13Myc::TRP1	yCH001